



Structural, Morphological and Optical Characteristics of Low Temperature Oxidized Metallic Zinc Films

K. U. Isah^{1*}, A. M. Ramalan¹ and B. J. Jolayemi¹

¹Department of Physics, Federal University of Technology, School of Physical Sciences, Minna, Nigeria.

Authors' contributions

This work was carried out in collaboration between all authors. Author KUI conceptualized and designed the research, he also conducted the morphological and structural analysis of the samples, author AMR carried out the samples preparation, wrote the initial draft and searched for relevant literatures. Author BJJ was involved in the analysis of the optical properties of the samples and the management and use of the relevant literatures for analysis. All authors read and approved the final manuscript.

Article Information

DOI: 10.9734/BJAST/2016/26853

Editor(s):

(1) Shahin Atashbar Tehrani, Particle Physics, Amirkabir University of Technology, Tehran, Iran.

Reviewers:

(1) Sutthipoj Sutthana, Kasetsart University, Thailand.

(2) Prasada Rao Talakonda, K L University, Andhra Pradesh, India.

(3) M. Zemzemi, University of Gabes, Tunisia.

(4) Richa Srivastava, Babasaheb Bhimrao Ambedkar University, Lucknow, India.

Complete Peer review History: <http://sciencedomain.org/review-history/15338>

Original Research Article

Received 6th May 2016
Accepted 20th June 2016
Published 9th July 2016

ABSTRACT

This work presents the effect of low temperature- below Zn melting point oxidation of Zn film on the optical, morphological and structural properties of thermally oxidized Zn films. Zinc oxide (ZnO) thin films were synthesised from thermal vacuum deposited metallic zinc thin films by low temperature thermal oxidation of the Zn films between 200°C and 400°C. The ZnO films exhibited preferred (011) orientation wurtzite structure, with presence of Zn peaks that diminishes with increase in the oxidation temperature. The films show modification in morphology exhibiting different nanostructures at different Zn film oxidation temperature. The stoichiometric ratio between Zn and O atoms of the ZnO films synthesized at oxidation temperature of 400°C show much closer value to the ideal 1:1 ratio giving ZnO_{0.94} while at 200 and 300°C oxidation temperature the deviation from ideal was more with stoichiometry of ZnO_{0.74}. The films had optical transmittance of 64-71% in the visible region with

*Corresponding author: E-mail: kasim309@futminna.edu.ng;

the transmission edge becoming sharper and the optical band gap improving from 2.90 to 3.30 eV with increase in oxidation temperature. The lattice parameter c/a ratio was ≈ 1.732 for all the samples, showing a deviation of 0.099 from the ideal 1.633 of wurtzite structure belonging to the space group P63mc by 0.099. The Zn-O bond length were ≈ 1.834 Å for each samples, which is also less than ideal 1.993 Å along c-axis an indication of the planes being more closely packed than the ideal. The refractive index dispersion of the ZnO films below the interband absorption edge were analyzed based on the single-oscillator model.

Keywords: Zinc oxide; thermal oxidation; surface morphology; XRD.

1. INTRODUCTION

ZnO is a II–VI compound semiconductor with ionicity between that of covalent and ionic semiconductors [1]. It is a wide band-gap (3.37 eV) compound semiconductor suitable for short wavelength optoelectronic applications [2]. ZnO has a large free-exciton binding energy that make excitonic emission processes persist at or even above room temperature [3]. It is a key technological material in optoelectronics, electronic, in the fabrication of devices such as blue and ultraviolet light-emitting diodes and lasers operational at high temperatures and extreme radiation conditions [4,5,6]. ZnO is also a versatile functional material with of growth various morphologies, such as nanocombs, nanorings, nanohelices/nanosprings, nanobelts, nanowires and nanocages, depending of deposition process [2] leading to wide range of promising applications.

Several techniques have been used to deposit ZnO thin films including sol-gel, solvothermal, sputtering, spray pyrolysis, molecular beam epitaxy, MOCVD, Magnetron sputtering and thermal oxidation [7]. Most of these are expensive and complicated techniques and some drawbacks, involving long reaction time, toxic templates and use of metal catalysts. Metallic Zn film have been deposited by cathodic vacuum arc, thermal evaporation, electron beam evaporation and sputtering [8-11]. High quality ZnO films have been synthesized by simple method involving the thermal oxidation of metallic Zn film [8] at high oxidation temperature. The synthesis ZnO by thermal oxidation of Zn films has the advantage of its simplicity, efficiency and low cost. Very little work has been reported on thermal oxidation of metallic Zn films at low temperature regime below Zn melting point of 419°C.

In this work, we present low temperature oxidation of Zn metallic films deposited by vacuum thermal evaporation. The

microstructural, morphological and optical properties of the films were investigated using X-ray diffraction (XRD), Field emission scanning electron microscope (FESEM), Atomic force microscope (AFM) and UV/Vis spectroscopy.

2. MATERIALS AND METHODS

Metallic zinc (Zn) pellets (99.9%) was evaporated onto glass substrate under vacuum from a molybdenum boat at substrate temperature of 150°C and constant deposition rate of 2 nm s^{-1} using an EDWARD Auto306 thermal evaporator with FL 400 deposition chamber to obtain Zn films of 150 nm thickness. The source to substrate distance was kept at 8 cm. After deposition, the metallic Zn precursor thin films were each oxidised in open air under atmospheric Pressure. The ZnO films were synthesised by thermally oxidising the Zn films in open air using a horizontal Carbolite 201 tubular furnace at temperatures 200°C, 300°C, and 400°C, the temperature ramping rate was 10°C/min. A dwelling time of 120 min was adopted to oxidise the films. The samples were labelled $T_{\text{oxid}_200^\circ\text{C}}$, $T_{\text{oxid}_300^\circ\text{C}}$ and $T_{\text{oxid}_400^\circ\text{C}}$ for metallic Zn films oxidised at 200, 300 and 400°C respectively.

The morphology of the films were investigated using JEOL JSM - 7600F Field Emission Scanning Microscopy (FESEM) equipped with an Aztec and INCA microanalysis system with 50 mm² silicon drift detector, as well as INCA wave wavelength dispersive spectrometer (WDS) system for elemental analysis and Atomic force microscope (AFM) using an XE-100 Park system attached with XE Series (SPM) Shidmadzu. The X-ray diffraction(θ – 2θ) diagrams were recorded with 2θ scanning from 25° to 60°, in step size 0.040° and a constant counting times of 3.17 s/step, and the generator settings of 40 mA and 42 kV, using CuK_α of 1.5406 Å using a X'Pert' Powder PANALYTICAL Bruker D8 Advance Diffractometer. The optical and vibrational properties were investigated using Avantes UV-

VIS spectrophotometer (AVASPEC 2048) in the wavelength range 250 - 900 nm and ProRaman-L ENWAVE OPTRONICS Raman spectrometer with 750 nm wavelength respectively.

3. RESULTS AND DISCUSSION

3.1 Structural Properties

X-ray diffraction (XRD) was used to identify the crystalline phases of the films. The XRD spectra of the synthesised are given in Fig. 1. It shows the oxidised metallic zinc films have similar crystalline phases.

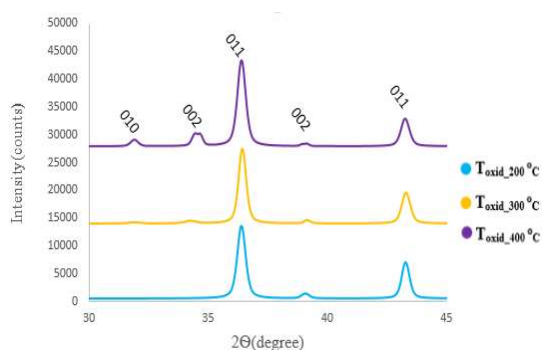


Fig. 1. XRD patterns of as-synthesised ZnO thin films at different oxidation temperatures: 200°C, 300°C and 400°C

All the samples present sharp diffraction peaks at $2\theta = 36.47^\circ$ indicating a dominant (011) texture of hexagonal ZnO structure, the peaks at 32.23° , 34.55° corresponding to (010), (002) planes respectively are also indexed to ZnO hexagonal (wurtzite) structure (ICSD 169463). The observed (002) and (011) peaks around 39.27° and 43.35° belongs to Zn hexagonal system of space group P63/mmc (ICSD 52259). The identified peaks which are associated with Zn hexagonal could originate from oxidised zinc atoms during the oxidation process [12]. The (010), (002 and (011) peaks of ZnO become pronounced with increase in oxidation temperature. The films are preferentially oriented along (011) direction rather than the usual (002) orientation, indicating growth of ZnO crystallites have preferential (011) plane at low oxidation temperatures below the melting point of Zn. The (010) and (002) ZnO peaks increased as oxidation temperature increased.

The structural parameters that characterise the ZnO at different oxidation temperatures are presented in Table 1.

The lattice parameters a and c for the ideal hexagonal wurtzite structure mostly range from 3.2475 to 3.2501 Å for the a -parameter and from 5.2042 to 5.2075 Å for the c -parameter [1]. The observed c parameters were 5.212 for $T_{\text{oxid}_200^\circ\text{C}}$ and $T_{\text{oxid}_400^\circ\text{C}}$ and 5.194 Å for $T_{\text{oxid}_300^\circ\text{C}}$, close to the ideal value. However the lattice parameter ' a ' show some deviation from the ideal for all samples. The ratio of the lattice parameter c/a had a constant value of ≈ 1.732 for all the samples, which is greater than that of ideal value of 1.633 [1] for wurtzite structure belonging to the space group P63mc by 0.099. Thus showing a slight deviation from ideal arrangement. These deviations are due to defects in the lattice structure.

The average crystallite size of the ZnO thin films were deduced using Debye Scherrer's formula [13].

$$D = \frac{0.9\lambda}{\beta \cos\theta}$$

Where β = full width at half maximum (FWHM), k (= 0.9) is the size factor, θ = diffraction angle at which the maximum intensity was observed, and λ = wavelength of the X-rays used (1.54060 Å) and D is crystallite size respectively. The values of D are given in Table 2.

The texture coefficient (TC) represents the texture of a particular plane, whose deviation from unity implies the preferred growth. The value $TC(hkl) = 1$ represents films with randomly oriented crystallites, while higher values indicate the abundance of grains oriented in a given (hkl) direction, TC , is given by Ong et al. [14],

$$TC_{hkl} = \frac{I_{hkl}/I_{o(hkl)}}{N^{-1} \sum I_{hkl}/I_{o(hkl)}}$$

The (002) texture $TC_{(002)}$, for $T_{\text{oxid}_200^\circ\text{C}}$ is characterized by a random crystallite orientation with $TC_{(002)}$ equals to unity as given in Table 2. The samples shows increasing $TC_{(002)}$ texture with increase in oxidation temperature. The texture coefficient for the (011) orientation of the samples have values greater than unity, between 1.4 at $T_{\text{oxid}_300^\circ\text{C}}$ and 2.8 at $T_{\text{oxid}_400^\circ\text{C}}$, this shows the nanocrystals have increasing texture in this orientation and large number of crystallites are oriented with the (011) planes parallel to substrate surface [15] with increase in oxidation temperature. The highest $TC_{(hkl)}$ was in (011) plane showing preferred (011) texture at the temperatures considered.

Table 1. Structural parameters for prominent orientation at different oxidation temperatures

hkl	T _{oxid_200°C}				T _{oxid_300°C}				T _{oxid_400°C}			
	2θ	a	c	c/a	2θ	a	c	c/a	2θ	a	c	c/a
002	34.39	3.009	5.212	1.732	34.51	2.999	5.194	1.732	34.39	3.009	5.212	1.732
011	36.35	2.852	4.939	1.732	36.38	2.850	4.936	1.732	36.35	2.852	4.939	1.732

Table 2. Crystallite size, texture coefficient and nearest-neighbour bond length of the ZnO films

hkl	T _{oxid_200°C}			T _{oxid_300°C}			T _{oxid_400°C}		
	D (nm)	TC	L (nm)	D (nm)	TC	L (nm)	D (nm)	TC	L (nm)
002	52.68	1.0	1.882	26.35	2.4	1.876	52.68	2.7	1.882
011	37.08	1.4		41.23	2.9		37.08	2.8	

The nearest-neighbour Zn-O bond length L along the c -direction was determined from the lattice parameters using [16],

$$L = \left[\frac{a^2}{3} + \left(\frac{1}{2} - u \right)^2 c^2 \right]^{1/2}$$

Where the parameter “ u ” defined as the length of the bond parallel to the c axis is given by

$$u = \frac{a^2}{3c^2} + 0.25$$

The values of the Zn-O bond lengths obtained were $\approx 1.834 \text{ \AA}$ for each sample as given in Table 2. This is less than the theoretical Zn-O bond length of 1.993 \AA along c -axis and 1.973 \AA in the other three directions of the tetrahedral arrangements of the nearest neighbours determined from bond overlap population between Bloch functions on an atomic basis expansion [17], an indication of the planes being more closely packed than ideal.

The deviation in c/a ratio and nearest-neighbour bond length L from the ideal wurtzite crystal is probably due to lattice stability and ionicity [1]. However, the same numerical values of c/a and L obtained for all the samples indicates identical crystal structures irrespective of Zn film oxidation temperature.

3.2 Surface Morphology and Compositional Analysis

The morphology of the resulting ZnO samples from the oxidations at 200°C , 300°C to 400°C of metallic Zn films were examined by FESEM and shown in Fig. 2.

Each oxidation temperature yields a particular surface morphology characteristic of that particular temperature. Fig. 2 (a) exhibits a hexagonal nanoplatelet-like shape at oxidation temperature of 200°C which transformed into nanorod/nanoarc-like nanostructures at 300°C as confirmed in Fig. 2 (b). Fig. 2 (c) displays nanoplatelet/nanoarc-like shapes at oxidation temperature of 400°C . These phase transformations may be attributed to the change in oxidation temperature. The average grain size obtained from the FESEM images were between 551.10 to 555.60 nm , given in Table 3.

Fig. 3 shows the EDX spectra of the samples it shows only Zn and O and no other element.

The Zn and O compositions of the samples are presented in Table 3. It shows that oxygen sufficiently reacts with the Zn films at 300 and 400°C resulting in an almost stoichiometric film of $\text{ZnO}_{0.94}$. While oxidation at 200°C yielded $\text{ZnO}_{0.73}$ exhibiting higher deviation from stoichiometry. This may be due to fewer effective diffusion paths for oxygen and thus efficient oxidation of the films as the oxidation of Zn film below the melting point of Zn (419°C) occurs through the diffusion of Zn atoms and oxygen atoms in the solid phase [18]. Rambu & Iftimie [19] reported achieving total oxidation of Zn films at a temperature of 300°C , the oxidation time being 2 hours.

The AFM images in 2D and 3D of ZnO thin films at different oxidation temperatures are presented in Fig. 4, these show the surface morphologies and topographies of ZnO thin films with respect to their oxidation temperatures.

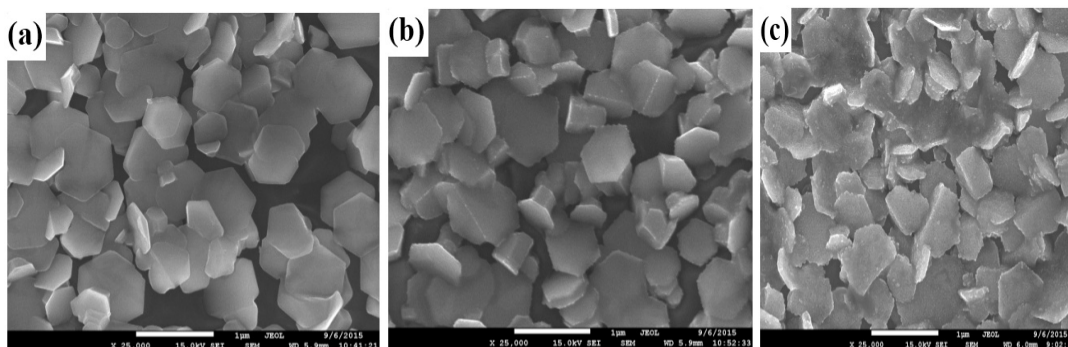


Fig. 2. FESEM images of ZnO at constant substrate temperature of 150°C and different oxidation temperatures: (a) 200°C (b) 300°C (c) and 400°C

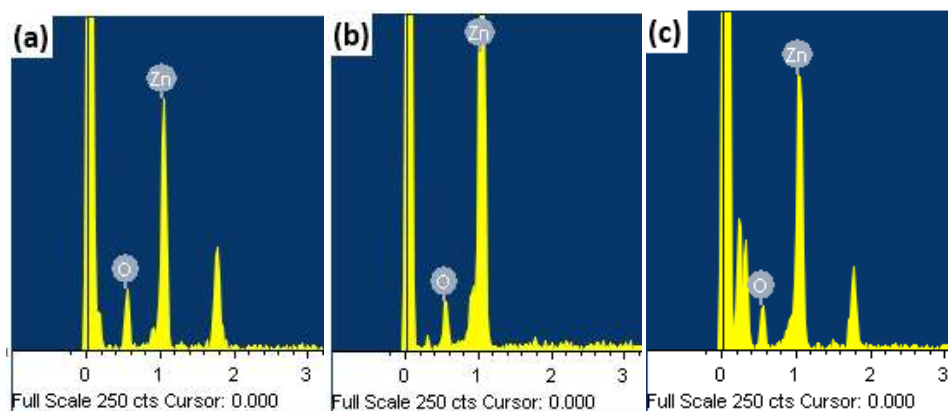


Fig. 3. EDX Spectra at different oxidation temperatures: (a) 200°C (b) 300°C (c) 400°C

Table 3. Effects of oxidation temperature on the chemical composition of ZnO thin film

Sample	Chemical composition at %			Grain size (nm)	R _a (nm)
	Zn	O	ZnO _x		
T _{oxid_200°C}	57.93	42.07	ZnO _{0.73}	555.60	46.39
T _{oxid_300°C}	51.66	48.34	ZnO _{0.94}	551.10	56.64
T _{oxid_400°C}	51.56	48.44	ZnO _{0.94}	554.10	40.05

The surface roughnesses were evaluated over an area. It is observed that with increase in oxidation temperature from 200 to 300°C, the surface average roughness increases from 46.387 to 56.635 nm and then decreases to 40.053 nm at 400°C as shown in Table 3.

3.3 Optical Properties

The optical transmittance spectra of the samples were plotted and presented in Fig. 5. The films samples exhibit high transmittance of 81% for the film oxidized at 400°C, while a much lower transmittance of less than 65% was observed for oxidation temperatures of 200°C and 300°C in visible region of the spectrum. Un-oxidized zinc acts as scattering centres for light and, consequently, the optical transmittance is low as observed for film oxidized at 200°C.

The film oxidized at 400°C show a sharp rise in transmission near the fundamental absorption edge, an indication of good crystallinity of the film. The film oxidized at 200°C show more of broad rise in its transmission through its fundamental absorption, this may be due to incomplete oxidation, grain-boundary discontinuity effects in the structure and lack of stoichiometry [20]. This study shows, at higher oxidation temperatures, most metallic atoms are oxidised with subsequent decrease of optical

scattering, reduction of crystallite boundary density and thus increase in the optical transmittance.

The optical band gap E_g of the samples were deduced from the relation [21].

$$(\alpha h\nu) = B(h\nu - E_g)^{1/2}$$

Where α is absorption coefficient at photon energy $h\nu$, B is a constant. The optical band gap E_g were determined, by extrapolating the linear part of $(\alpha h\nu)^2$ versus $h\nu$ to $h\nu$ axis as shown in Fig. 6.

The optical band gaps determined were 2.90, 3.02 and 3.30 eV for samples T_{oxid_200°C}, T_{oxid_300°C} and T_{oxid_400°C} respectively. This shows increase in band gap with increasing oxidation temperature from 2.90 eV at 200°C oxidation temperature to 3.30 eV at oxidation temperature of 400°C. The optical band gap at oxidation temperature of 400°C is in close agreement with 3.37 eV for bulk ZnO [22] as a result of near complete oxidation of the Zn films at this temperature. The band gaps at 200 and 300°C are quite less than 3.37 eV and can be attributed to the greater density of donor state near the conduction band determined by the oxygen vacancies [19].

The dispersion of the refractive index (n) were evaluated according to the single oscillator model proposed by Wemple-DiDomenico as [23],

$$n^2 - 1 = \frac{E_d E_o}{(E_o^2 - E^2)}$$

where n is the refractive index, E_o and E_d are single oscillator parameters, E_o is the energy of the effective dispersion oscillator, E_d is the dispersion energy, which measures the intensity of the inter band optical transitions while E is photon energy.

Fig. 7 shows a plot of (n²-1) versus (hv)² from which the, E_g and E_d were estimated from the slope (E_oE_d)⁻¹ and the intercept on the vertical axis, (E_o/E_d).

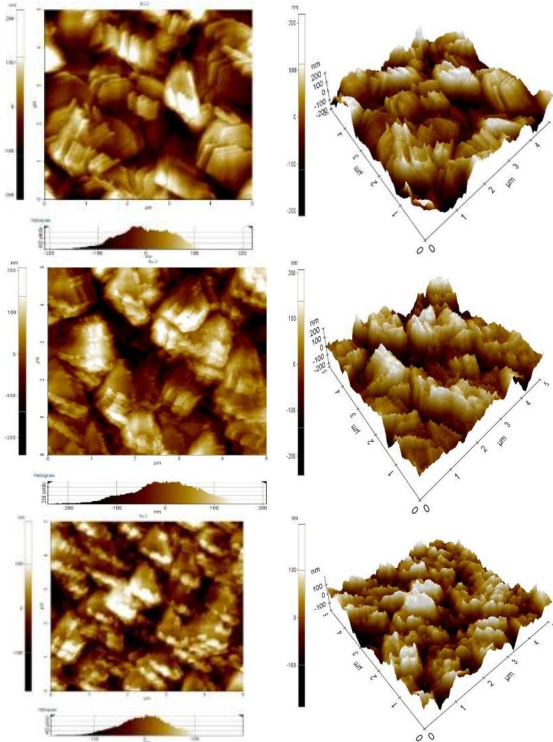


Fig. 4. 2D and 3D Morphological Images of ZnO films at (a) 200°C Oxidation Temperature, (b) 300°C and (c) 400°C

Table 4 shows the values obtained for E_o and E_d of the films. The oscillator energy E_o decreased with increase in oxidation temperature, with lowest value of 2.60 eV at T_{oxid_300°C}. E_d decrease with increasing oxidation temperature.

The ratio of E_o/E_g was between 0.86 and 1.92, Zhaoyang and Lizhong [24] got an empirical relationship E_o/E_g ≈ 2 for PLD deposited ZnO films, while an empirical relation of E_o/E_d ≈ 1.5 was reported by Ziabari and Ghodsi for sol-gel derived CdS films [25]. E_o generally obeys an empirical relationship E_o ≈ 2E_g [26,27].

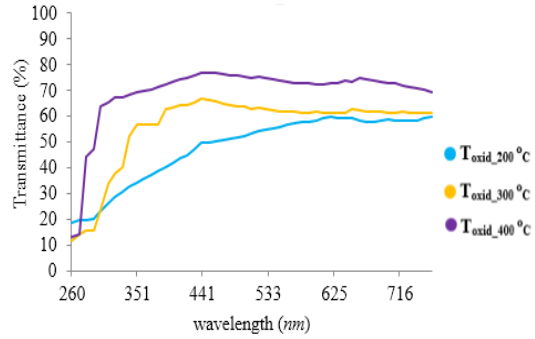


Fig. 5. Transmittance spectra over wavelength as a function of oxidation temperature

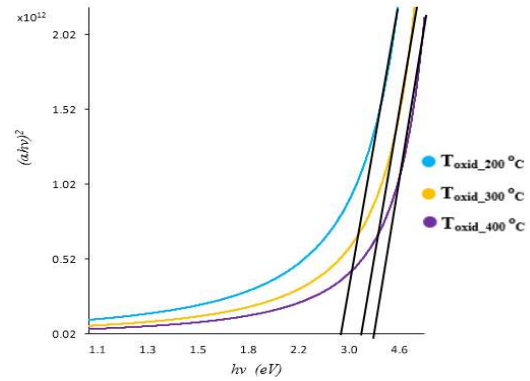


Fig. 6. Extrapolation of optical bandgap of as-synthesised ZnO thin films at different oxidation temperatures

Table 4. Oscillator model parameter summary at different oxidation temperature

Oxidation temperature (°C)	E _d (eV)	E _o (eV)	E _g (eV)	E _o /E _g
T _{oxid_200°C}	6.07	5.56	2.90	1.92
T _{oxid_300°C}	6.81	2.60	3.02	0.86
T _{oxid_400°C}	5.26	3.55	3.30	1.10

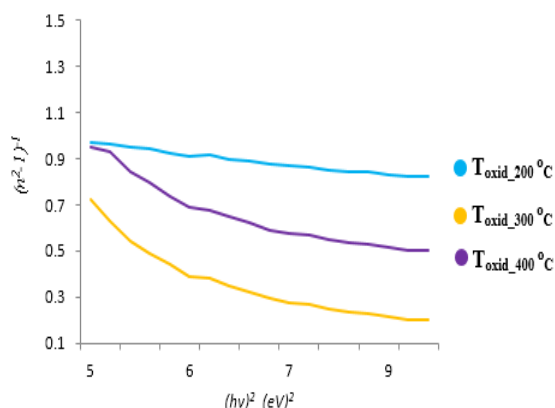


Fig. 7. Single oscillator model variation with oxidation temperature

4. CONCLUSION

ZnO films were synthesized from low temperature oxidation of metallic Zn films. The films were preferentially oriented along (011) direction with (010) and (002) peaks of ZnO increasing with increase in oxidation temperature. The ratio of the lattice parameter c/a had a constant value of ≈ 1.732 for all the samples showing a slight deviation from ideal of 1.633 for ZnO. The Zn films oxidised at 300 and 400°C resulted in an almost stoichiometric film of ZnO_{0.94}. While oxidation at 200°C yielded ZnO_{0.73} exhibiting higher deviation from stoichiometry as a result of fewer effective diffusion path for oxygen at lower oxidation temperature. The optical band gap was between 2.90 eV at 200°C oxidation temperature and 3.3 eV at 400°C, which show an increasing improvement towards standard ZnO band gap of 3.37 eV with increase in oxidation temperature.

Analysis of the refractive index dispersion relation using the single-oscillator model shows E_d the dispersion energy, which measures the intensity of the inter band optical transitions decreased with increase in oxidation temperature. Thermal oxidation can be a promising method to obtain ZnO transparent conducting thin films for different technological applications.

COMPETING INTERESTS

Authors have declared that no competing interests exist.

REFERENCES

1. Morkoç H, Özgür U. Zinc oxide: Fundamentals, materials and device technology, Verlag: Wiley-VCH; 2009.
2. Wang ZL. Zinc oxide nanostructures: Growth, properties and applications. *J Phys Condens Matter*. 2004;16:R829–R858.
3. Reynolds DC, Look DC, Jogai B. Optically pumped ultraviolet lasing from ZnO. *Solid State Commun*. 1996;99(12):873-875.
4. Tang ZK, Wong GKL, Yu P, Kawasaki M, Ohtomo A, Koinuma H, Segawa Y. Room-temperature ultraviolet laser emission from self-assembled ZnO microcrystallite thin films. *Appl Phys Lett*. 1998;72(25):3270-3272.
5. Zu P, Tang ZK, Wong GKL, Kawasaki M, Ohtomo A, Koinuma H, Segawa Y. Ultraviolet spontaneous and stimulated emissions from ZnO microcrystallite thin films at room temperature. *Solid State Commun*. 1997;103(8):459-463.
6. Look DC, Claflin B. P-type doping and devices based on ZnO. *Phys Status Solidi B Basic Solid State Phys*. 2004;240(3): 624–630.
7. Kumar K, Kumar G, Al-Dossary O, Umar A. ZnO nanostructured thin films: Depositions, properties and applications—A review. *Mater Express*. 2015;5(1):3-23.
8. Cho S, Ma J, Kim Y, Sun Y, Wong GKL, Ketterson JB. Photoluminescence and ultraviolet lasing of polycrystalline ZnO thin films prepared by the oxidation of the metallic Zn. *Appl Phys Lett*. 1999;75(18): 2761-2763.
9. Kim T-W, Kawazoe T, Yamazaki S, Lim J, Yatsui T, Ohtsu M. Room temperature ultraviolet emission from ZnO nanocrystallites fabricated by the low temperature oxidation of metallic Zn precursors. *Solid State Commun*. 2003;127(1):21-24.
10. Gupta RK, Shridhar N, Katiyar M. Structure of ZnO films prepared by oxidation of metallic Zinc. *Mater Sci Semicond Process*. 2002;5(1):11-15.
11. Alivov YI, Chernykh A, Chukichev A, Korotkov RY. Thin polycrystalline zinc oxide films obtained by oxidation of metallic zinc films. *Thin Solid Films*. 2005;473:241–246.

12. Li C, Li X, Wang D. Fabrication of ZnO thin film and nanostructures for optoelectronic device applications. In: Mele P, Endo T, Arisawa S, Li C, Tsuchiya T. Oxide thin films, multilayers, and nanocomposites. Cham, Switzerland: Springer International Publishing. 2015;239-272.
13. Klug HP, Alexander L. X-ray diffraction procedures for polycrystalline and amorphous materials. New York: John Wiley and Sons; 1974.
14. Ong HC, Zhu AXE, Du GT. Dependence of the excitonic transition energies and mosaicity on residual strain in ZnO thin films. Appl Phys Lett. 2002;80(6):941-943.
15. Márquez JAR, Rodríguez CMB, Herrera CM, Rosas ER, Angel Z, Pozos OOT. Effect of surface morphology of ZnO electrodeposited on photocatalytic oxidation of methylene blue dye. Int J Electrochem Sci. 2011;6:4059-4069.
16. Ambacher O, Majewski J, Miskys C, Link A, Hermann M, Eickhoff M, Stutzmann M, Bernardini F, Fiorentini V, Tilak V, Schaff B, Eastman LF. Pyroelectric properties of Al(In)GaN/GaN heteroand quantum well structures. J Phys Condens Matter. 2002;14(13):3399–3434.
17. Yu ZX, Zhou-Wen C, Yan-Pen Q, Yan F, Liang Z, Li Q, Ming-Zhan MA, Ri-Ping L, Wen-Kui W. An initio comparative study of Zincblende and Wurtzite ZnO. Chin Phys Lett. 2007;24(4):1032-1034.
18. Lee G-H. Relationship between crystal structure and photoluminescence properties of ZnO films formed by oxidation of metallic Zn. Electron Mater Lett. 2010;6(4):155-159.
19. Rambu AP, Iftimie N. Synthesis and characterization of thermally oxidized ZnO films. Bull Mater Sci. 2014;37(3):441–448.
20. Pawar SH, Bhosale PN, Uplane MD, Tamhankar S. Growth of Bi₂S₃ film using a solution-gas interface technique. Thin Solid Films. 1983;110(2):165-170.
21. Lan W, Liu Y, Zhang M, Wang B, Yan H, Wang Y. Structural and optical properties of La-doped ZnO films prepared by magnetron sputtering. Mater Lett. 2007;61(11-12):2262-2265.
22. Rusu GG, Rambu AP, Rusu M. On the optical properties of heat-treated multilayered Zn/In thin films. J Optoelectron Adv Mater. 2008;10(2):339-343.
23. Wemple S, Didomenico VJ. Behavior of the electronic dielectric constant in covalent and ionic materials. Phys Rev B. 1971;3(4):1338-1351.
24. Zhaoyang W, Lizhong H. Effect of oxygen pressure on the structural and optical properties of ZnO thin films on Si (111) by PLD. Vacuum. 2009;83(5):906-909.
25. Ziabari AA, Ghodsi FE. Growth, characterization and studying of sol–gel derived CdS nanocrystalline thin films incorporated in polyethyleneglycol: Effects of post-heat treatment. Sol Energy Mater Sol Cells. 2012;105:249–262.
26. Goldsmith S, Cetinorgu E, Boxman R. Modeling the optical properties of tin oxide thin films. Thin Solid Films. 2009;517(17): 5146-5150.
27. You Z Z and Hua G J. Refractive index, optical bandgap and oscillator parameters of organic films deposited by vacuum evaporation technique. Refractive index, optical bandgap and oscillator parameters of organic films deposited by vacuum evaporation technique. Vacuum. 2009; 83(16):984-988.

© 2016 Isah et al.; This is an Open Access article distributed under the terms of the Creative Commons Attribution License (<http://creativecommons.org/licenses/by/4.0>), which permits unrestricted use, distribution, and reproduction in any medium, provided the original work is properly cited.

Peer-review history:
The peer review history for this paper can be accessed here:
<http://sciencedomain.org/review-history/15338>